2016

A discontinuous Galerkin method for unsteady two-dimensional convective flows

Andreas C. Aristotelous
West Chester University of Pennsylvania, aaristotelous@wcupa.edu

N. C. Papanicolaou
University of Nicosia

Recommended Citation
Aristotelous, A. C., & Papanicolaou, N. C. (2016). A discontinuous Galerkin method for unsteady two-dimensional convective flows. *AIP Conference Proceedings, 1773*(110002), 110002-1-110002-12. http://dx.doi.org/10.1063/1.4965006

A discontinuous Galerkin method for unsteady two-dimensional convective flows

A. C. Aristotelous' and N. C. Papanicolaou'

Citation: AIP Conference Proceedings **1773**, 110002 (2016); doi: 10.1063/1.4965006
View online: http://dx.doi.org/10.1063/1.4965006
View Table of Contents: http://aip.scitation.org/toc/apc/1773/1
Published by the American Institute of Physics

A Discontinuous Galerkin Method for Unsteady Two-dimensional Convective Flows

A. C. Aristotelous[1,b)] and N. C. Papanicolaou[2,a)]

[1]*Dept. of Mathematics, West Chester University, 25 University Ave, West Chester, PA 19383, USA*
[2]*Dept. of Mathematics, University of Nicosia, P.O. Box 24005, 1700 Nicosia, Cyprus*

[a)]Corresponding author: papanicolaou.n@unic.ac.cy
[b)]aaristotelous@wcupa.edu

Abstract. We develop a High-Order Symmetric Interior Penalty (SIP) Discontinuous Galerkin (DG) Finite Element Method (FEM) to investigate two-dimensional in space natural convective flows in a vertical cavity. The physical problem is modeled by a coupled nonlinear system of partial differential equations and admits various solutions including stable and unstable modes in the form of traveling and/or standing waves, depending on the governing parameters. These flows are characterized by steep boundary and internal layers which evolve with time and can be well-resolved by high-order methods that also are adept to adaptive meshing. The standard no-slip boundary conditions which apply on the lateral walls, and the periodic conditions prescribed on the upper and lower boundaries, present additional challenges. The numerical scheme proposed herein is shown to successfully address these issues and furthermore, large Prandtl number values can be handled naturally. Discontinuous source terms and coefficients are an innate feature of multiphase flows involving heterogeneous fluids and will be a topic of subsequent work. Spatially adaptive Discontinuous Galerkin Finite Elements are especially suited to such problems.

INTRODUCTION

The main purpose of the current work is to provide a stepping stone towards the development of a reliable numerical framework for the solution of complex convective flow problems with added features, such as multiphase flows [1], biological fluids [2] and nutrient/gas solutions [3]. These flows will be investigated in both a constant- and a micro-gravity [4, 5] environment. In addition, the effect of applying the Maxwell-Cattaneo heat conduction law [6, 7, 8, 9, 10] to the system will also be investigated.

In order to be able to tackle the aforementioned problems we first need to have a robust, accurate and efficient numerical scheme. The problem of unsteady two-dimensional flow subject to a vertical temperature gradient provides an excellent benchmark for developing and testing our method, since it contains many of the features we seek to address, such as a coupled nonlinear system subject to different types of boundary conditions, e.g. periodic and no-slip.

This flow and its variants have been the topic of numerous works. The linear stability was examined experimentally, theoretically and numerically in the classic works of Elder [11], Gill and Davey [12] and Bergholz [13] listed in chronological order. Christov and Homsy [14] extended the analysis to include the nonlinear dynamics of the flow with and without gravity modulation with the aid of an energy-conservative finite-difference splitting scheme and Christov and Tang in [15] investigated the constant gravity case further using the same scheme.

The case of plane-parallel convective flow under g-jitter was examined in [16] with the aid of a Beam-Galerkin Spectral method and the same method was applied to investigate the effect of the Maxwell-Cattaneo heat conduction law on one-dimensional-in-space g-jitter convective flows subject to two thermal gradients [17].

In a previous work [18], we revisited the problem of two-gradient convection, where an SIP-DG Finite Element scheme was developed for the case of plane parallel flow in streamfunction-vorticity formulation. The results were found to be in good agreement with [17]. Note that for the case of plane-parallel flow, the problem is linear and no periodic boundary conditions are required. Here, we extend our previous work to two spatial dimensions including nonlinearities and the periodic portion of the boundary.

Application of Mathematics in Technical and Natural Sciences
AIP Conf. Proc. 1773, 110002-1–110002-12; doi: 10.1063/1.4965006
Published by AIP Publishing. 978-0-7354-1431-0/$30.00

THE TWO-DIMENSIONAL CONVECTIVE FLOW

Flow Geometry

Consider the two-dimensional convective flow in an infinite vertical slot of width L with an imposed linear vertical temperature gradient and differentially heated lateral walls (see ref [14, 16]) as depicted in Figure 1. Following standard notation, u and v are the x- and y-components of the velocity vector $\boldsymbol{u}$, ψ is the vorticity stream function defined by $u = \partial\psi/\partial y$, $v = -\partial\psi/\partial x$, ν is the kinematic viscosity, κ the thermal diffusivity, T the temperature and β the coefficient of volumetric expansion. The temperatures of the left and right walls at $y = 0$ are denoted by T_L^* and T_R^* respectively, $\delta T = T_L^* - T_R^*$ is the horizontal temperature difference and τ_B is the vertical temperature gradient.

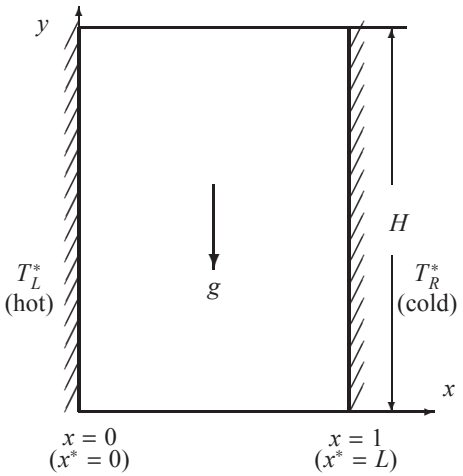

FIGURE 1. The flow geometry for the convective problem

Denoting dimensional variables with an asterisk and adopting the scheme introduced in [14] we define the dimensionless variables

$$x = \frac{x^*}{L}, \quad y = \frac{y^*}{L}, \quad t = t^* \frac{\kappa}{L^2}, \quad \psi = \frac{\psi^*}{\kappa}, \quad \theta = \frac{T^*}{\delta T} - \frac{1}{2} - \tau_B y, \quad \tau_B = \frac{\tau_B^* L}{\delta T}. \tag{1}$$

It is important to note here that the dimensionless temperature θ is the departure from the linear vertical stratification. Also, in accordance with theory and experimental observations (see, *e.g.*, [13]), the perturbation solutions are periodic in the vertical direction. The dimensionless wavelength of the periodic solutions is denoted by $H = 2\pi/\alpha$ where α is the wavenumber.

The dimensionless parameters Ra and Pr are termed the Rayleigh and Prandtl numbers and are given by

$$\mathrm{Ra} = \frac{\beta g_0 \delta T L^3}{\nu\kappa} \quad \text{and} \quad \mathrm{Pr} = \frac{\nu}{\kappa}, \tag{2}$$

respectively. In addition, the stratification parameter γ is defined by $4\gamma^4 = \tau_B \mathrm{Ra}$. Its significance will be discussed later.

If the slot is placed in a microgravity environment, which will be discussed in a future work, the body force g acting in the negative y-direction is harmonic, namely,

$$g = g_0(1 + \varepsilon \cos \Omega t), \tag{3}$$

where g_0 is the mean gravity, ε and Ω are the g-jitter amplitude and cyclic frequency respectively and t is the time.

Governing Equations

The 2-D convective flow is governed by the coupled nonlinear initial boundary value problem (IBVP)

$$\frac{1}{\mathrm{Pr}}\frac{\partial \Delta\psi}{\partial t} + \frac{1}{\mathrm{Pr}} J(\psi, \Delta\psi) = -\mathrm{Ra}\frac{\partial \theta}{\partial x} + \Delta^2\psi, \tag{4}$$

$$\frac{\partial \theta}{\partial t} + J(\psi, \theta) - \tau_B \frac{\partial \psi}{\partial x} = \Delta\theta, \tag{5}$$

where $J(u, v) = u_y v_x - u_x v_y$ is the nonlinear operator and u, v any two differentiable functions. System (4)-(5) is subject to boundary conditions in the x-direction

$$\begin{aligned} \psi = \frac{\partial \psi}{\partial x} = 0\,, \quad \theta = \frac{1}{2} \qquad \text{for} \quad x = 0, \\ \psi = \frac{\partial \psi}{\partial x} = 0\,, \quad \theta = -\frac{1}{2} \qquad \text{for} \quad x = 1, \end{aligned} \tag{6}$$

and periodic conditions in the y-direction

$$\begin{gathered} \psi(x, 0, t) = \psi(x, H, t),\ \ \psi_y(x, 0, t) = \psi_y(x, H, t) \\ \psi_{yy}(x, 0, t) = \psi_{yy}(x, H, t),\ \ \psi_{yyy}(x, 0, t) = \psi_{yyy}(x, H, t), \\ \theta(x, 0, t) = \theta(x, H, t),\ \ \theta_y(x, 0, t) = \theta_y(x, H, t). \end{gathered} \tag{7}$$

Note that the streamfunction formulation was employed in order to eliminate the pressure reducing the number of unknown functions and partial differential equations.

THE NUMERICAL METHOD

Notation and Preliminaries

For a regular domain D, $(\cdot, \cdot)_D$ is the inner product on $L^2(D)$, and $\langle \cdot, \cdot \rangle_{\partial D}$ denotes the inner product on $L^2(\partial D)$.

$\mathcal{T}_h = \{K\}$ defines a family of star-like partitions (triangulations) of the domain Ω parameterized by $0 < h < 1$. The weak formulations and the approximations involve functions that are discontinuous across interior boundaries, therefore, our functions belong to the "broken" Sobolev spaces

$$H^m(\mathcal{T}_h) = \prod_{K \in \mathcal{T}_h} H^m(K). \tag{8}$$

Note that members of these spaces are not functions in the proper sense since they can be multivalued on the interelement boundaries and can be interpreted as traces. Another consequence of the discontinuous nature of the functions is that the edges of the partition $\mathcal{T}_h$ play a prominent role in the formulation of the methods. So we define

$$\begin{aligned} \mathcal{E}^I &:= \text{ set of all interior edges of } \mathcal{T}_h, \\ \mathcal{E}^B &:= \text{ set of all boundary edges of } \mathcal{T}_h, \\ \mathcal{E} &:= \mathcal{E}^I \cup \mathcal{E}^B = \text{ set of all edges of } \mathcal{T}_h. \end{aligned}$$

For $e \in \mathcal{E}^I$, we have $e = \partial K^+ \cap \partial K^-$ for some $K^+, K^- \in \mathcal{T}_h$. Suppose $v \in E_h$. For $e \in \mathcal{E}^I$, we define the *jump* $[v]$ of v on e as $[v]|_e = v^+|_e - v^-|_e$ where v^+ and v^- denote the restrictions of v to K^+ and K^-, respectively. For $e \in \mathcal{E}^B$, we set $[v]|_e = v|_e$. For $e \in \mathcal{E}^I$ we define the *average* of v on e to be $\{v\}|_e := \frac{1}{2}(v^+|_e + v^-|_e)$. If $e \in \mathcal{E}^B$, set $\{v\}|_e = v|_e$. For $e \in \mathcal{E}$, h_e will denote the length of e when $n = 2$. For $e \in \mathcal{E}^I$, we define ∂_n as the normal derivative operator on e pointing from K^+ to K^-. For $e \in \mathcal{E}^B$, we define ∂_n in the same way, with the understanding that the unique cell containing e is labeled as K^+, there being no K^- for such edges.

For any $K \in \mathcal{T}_h$ and integer $r \geq 1$, let $\mathcal{P}_{r-1}(K)$ denote the set of all polynomials of degree less than or equal to $r - 1$ on K. The discontinuous finite element space V_h is defined by

$$V_h := \prod_{K \in \mathcal{T}_h} \mathcal{P}_{r-1}(K) \subset L^2(\Omega).$$

The maximum polynomial degree will be denoted $q := r - 1$; thus $r = q + 1$.

Numerical Scheme

In this section we present our numerical discretization scheme. The SIP-DG method is used for the spatial discretization. An important feature of this method is that it yields block symmetric positive definite linear algebraic systems which can be solved using efficient direct and iterative numerical solvers, *e.g.*, sparse Cholesky and Preconditioned CG methods based on multigrid with block smoothing. Treating the biharmonic in primal formulation results in a positive definite system unlike mixed formulation approaches [18], [19].

Since we do not need the introduction of an extra unknown, *e.g.*, the vorticity in this case, the resulting algebraic system has a smaller dimension compared to the one obtained from a mixed-formulation. In addition, it maintains its symmetry which is no longer the case for the block systems for ψ in [18], [19]. For optimal spatial accuracy a choice of degree $q \geq 3$ of basis functions is required. Nonetheless, having to use higher order polynomials to obtain optimal spatial accuracy does not necessarily affect the efficiency of the scheme. The resulting systems for the same accuracy are smaller, can exploit symmetry to save storage and faster solvers exploiting the positive definiteness and blocked nature of the system, can be employed.

The fully discrete SIP-DG weak formulation of our governing equations (4)-(5) subject to boundary conditions (6)-(7) as applied to the 2-D problem reads:

Find $\psi_h^n, \theta_h^n \in V_h$ such that

$$-\alpha_h^{PN}(\delta_n \psi_h, v) - \mathrm{Pr}\, \alpha_h^{PBih}(\psi_h^n, v) = -\mathrm{RaPr}\left(\frac{\partial \theta_h^{n-1}}{\partial x}, v\right) - \left(J(\psi_h^n, \Delta\psi_h^n), v\right), \quad \forall v \in V_h \tag{9}$$

$$(\delta_n \theta_h, v) + \alpha_h^{PD}(\theta_h^n, v) = \tau_B \left(\frac{\partial \psi_h^n}{\partial x}, v\right) + BT_h^{\theta}(\theta_h^n) - \left(J(\psi_h^n, \theta_h^n), v\right), \quad \forall v \in V_h \tag{10}$$

where the operator δ_n is the discrete time derivative defined in (14), and

$$BT_h^{\theta}(\theta_h^n) = -\sum_{e \in \mathcal{E}^B} \left\{ \left\langle \theta_h^n, \partial_n v \right\rangle_e - \gamma h_e^{-1} \left\langle \theta_h^n, v \right\rangle_e \right\}$$

is the weakly imposed Dirichlet boundary condition term for the temperature equation. The superscripts n and $n-1$ denote the current and previous time-steps respectively.

In our model and numerical implementation we require periodic conditions on the upper and lower parts of the boundary. It is very important to note here that the periodic boundary conditions for the second and fourth order equations are *implemented weakly* following the ideas in [20] for the Poisson equation. This is consistent with the classic DG formulations and the principal behind Discontinuous Galerkin methods.

The method proposed by Vemaganti in [20] requires the existence of the same number of edges in corresponding periodic boundaries and suggests the creation of a map between matching periodic edges, $e_i,\ e_j \in \mathcal{E}^B$, defined as periodic pairs e_p, that is, $e_p := \{e_i, e_j\}$, where $e_i \subseteq [0,1] \times \{y = 0\}$ and $e_j \subseteq [0,1] \times \{y = H\}$ and $\mathcal{E}^p$ is the set of all periodic pairs. Essentially, a periodic pair is treated as a single interior edge and the corresponding extra terms are introduced in the bilinear forms. When dealing with adaptive meshes there is a level of complexity in correctly maintaining the periodic map due to the fact that refined periodic edges may create an imbalance to the number of edges on each periodic boundary. This was addressed in our work and we provide a numerical test in a subsequent section.

The symmetric bilinear forms, $\alpha_h^{PD}(\cdot,\cdot)$, $\alpha_h^{PN}(\cdot,\cdot)$, incorporating the aforementioned periodic boundary conditions, corresponding to the Laplace operators, for Dirichlet, and Neumann conditions respectively, on the left and right parts

of the boundary, were inspired by [21, 22],

$$\begin{aligned}\alpha_h^{PD}(u_h,v) := &\sum_{K\in\mathcal{T}_h}(\nabla u_h,\nabla v)_K - \sum_{e\in\mathcal{E}^I}\left\{\langle\{\partial_n u_h\},[v]\rangle_e + \langle[u_h],\{\partial_n v\}\rangle_e - \gamma h_e^{-1}\langle[u_h],[v]\rangle_e\right\}\\ &- \sum_{e_p\in\mathcal{E}^P}\left\{\langle\{\partial_n u_h\},[v]\rangle_{e_p} + \langle[u_h],\{\partial_n v\}\rangle_{e_p} - \gamma h_e^{-1}\langle[u_h],[v]\rangle_{e_p}\right\} \qquad (11)\\ &- \sum_{e\in\mathcal{E}^B}\left\{\langle\partial_n u_h, v\rangle_e + \langle u_h,\partial_n v\rangle_e - \gamma h_e^{-1}\langle u_h, v\rangle_e\right\},\\ \alpha_h^{PN}(u_h,v) := &\sum_{K\in\mathcal{T}_h}(\nabla u_h,\nabla v)_K - \sum_{e\in\mathcal{E}^I}\left\{\langle\{\partial_n u_h\},[v]\rangle_e + \langle[u_h],\{\partial_n v\}\rangle_e - \gamma h_e^{-1}\langle[u_h],[v]\rangle_e\right\}\\ &- \sum_{e_p\in\mathcal{E}^P}\left\{\langle\{\partial_n u_h\},[v]\rangle_{e_p} + \langle[u_h],\{\partial_n v\}\rangle_{e_p} - \gamma h_e^{-1}\langle[u_h],[v]\rangle_{e_p}\right\}. \qquad (12)\end{aligned}$$

The symmetric bilinear form, $\alpha_h^{PBih}(u_h,v)$, for the biharmonic operator with essential boundary conditions on the non-periodic boundary, is given by,

$$\begin{aligned}\alpha_h^{PBih}(u_h,v) := &\sum_{K\in\mathcal{T}_h}(\Delta u,\Delta v)_K + \sum_{e\in\mathcal{E}}\{\langle\{\partial_n\Delta u\},[v]\rangle_e + \langle[u],\{\partial_n\Delta v\}\rangle_e\\ &- \langle\{\Delta u\},[\partial_n v]\rangle_e - \langle[\partial_n u],\{\Delta v\}\rangle_e + \gamma h_e^{-1}\langle[\partial_n u],[\partial_n v]\rangle_e + \gamma h_e^{-3}\langle[u],[v]\rangle_e\}\\ &+ \sum_{e\in\mathcal{E}^P}\{\langle\{\partial_n\triangle u\},[v]\rangle_{e_p} + \langle[u],\{\partial_n\Delta v\}\rangle_{e_p}\\ &- \langle\{\Delta u\},[\partial_n v]\rangle_{e_p} - \langle[\partial_n u],\{\Delta v\}\rangle_{e_p} + \gamma h_e^{-1}\langle[\partial_n u],[\partial_n v]\rangle_{e_p} + \gamma h_e^{-3}\langle[u],[v]\rangle_{e_p}\},\ \forall\, v\in V_h. \qquad (13)\end{aligned}$$

The bilinear form is an adaptation of the expressions that appear in [23, 24, 25] to incorporate the periodic portion of the boundary.

For the time-stepping, θ-method is employed, where we use λ as the parameter to avoid confusion with the temperature, *i.e.*,

$$\delta_n A^n = A^{n,\lambda} := \lambda A^n + (1-\lambda)A^{n-1},\ A\in\{t,\psi,\Delta\psi,\theta\}\ ,\quad 0<\lambda\le 1 \qquad (14)$$

As is well known $\lambda = 0$ and $\lambda = 1$ correspond to the explicit and implicit Euler methods respectively which provide o first-order approximation in time, whereas choosing $\lambda = 1/2$ corresponds to the Crank-Nicolson method which provides a second-order time scheme for the linear problem.

We obtain the following algebraic system

$$\begin{aligned}\left[\mathsf{S}^{\mathsf{N}}\boldsymbol{\psi^n} + \lambda\mathrm{Pr}\Delta t\,\mathsf{S}^{\mathsf{Bih}}\right]\boldsymbol{\psi^n} = &\left[\mathsf{S}^{\mathsf{N}} - (1-\lambda)\mathrm{Pr}\Delta t\,\mathsf{S}^{\mathsf{Bih}}\right]\boldsymbol{\psi^{n-1}} + \mathrm{RaPr}\boldsymbol{\partial_x\theta^{n-1}} \qquad (15)\\ &+ \lambda\Delta t\,\boldsymbol{J(\psi^n,\Delta\psi^n)} + (1-\lambda)\Delta t\,\boldsymbol{J}\left(\boldsymbol{\psi^{n-1},\Delta\psi^{n-1}}\right)\\ \left[\mathsf{M} + \lambda\Delta t\mathsf{S}^{\mathsf{D}}\right]\boldsymbol{\theta^n} = &\left[\mathsf{M} - (1-\lambda)\Delta t\mathsf{S}^{\mathsf{D}}\right]\boldsymbol{\theta^{n-1}} - \lambda\Delta t\,\boldsymbol{J(\psi^n,\theta^n)} - (1-\lambda)\Delta t\,\boldsymbol{J}\left(\boldsymbol{\psi^{n-1},\theta^{n-1}}\right) \qquad (16)\end{aligned}$$

where M is the block-diagonal symmetric positive-definite mass matrix given by $M_{ij} := (v_j, v_i)$, $S_{ij}^D := \alpha_h^{PD}(v_j,v_i)$ and $S_{ij}^N := \alpha_h^{PN}(v_j,v_i)$ are the block-structured symmetric positive- and semi-positive-definite stiffness matrices due to the discretization of the Laplacian. The symmetric positive definite matrix $\mathsf{S}^{\mathsf{Bih}} := \alpha_h^{PBih}(v_j,v_i)$ is the matrix corresponding to the biharmonic operator, where $i,j = 1,\ldots,M$ and M is the number of degrees of freedom in $\mathcal{T}_h$.

Implementation

We decouple equations (15), (16) by considering the partial derivative of θ in the right hand side of (15) at the previous time step. Therefore, we can solve two equations consecutively allowing for a different number of nonlinear iterations for each equation and thus increasing efficiency. Here, the nonlinear systems are solved in each time step using a fixed-point iteration and the iterations are terminated when the following Cauchy convergence criterion is satisfied

$$\frac{\max_{K\in\mathcal{T}_h}\|\boldsymbol{u_h^{n,[k]}} - \boldsymbol{u_h^{n,[k-1]}}\|_{L^2(K)}}{\max_{K\in\mathcal{T}_h}\|\boldsymbol{u_h^{n,[k]}}\|_{L^2(K)}} \le 10^{-10},$$

where $[k]$ and $[k-1]$ are the current and previous fixed-point-iteration steps and n is the current time step.

The block positive definite nature of our solution matrices allows us to solve the resulting linearized system (15), (16) using a sparse Cholesky solver which requires half the operations and half the storage compared to its LU counterpart. In the case of adaptive meshes, we use an iterative solver based on the preconditioned conjugate gradient method, exploiting once again the symmetry and positive definiteness of our operators and the blocked structure of the system to implement an efficient matrix-vector multiplication routine. The various matrices in the non-adaptive case, need only be assembled and factored once at the initial time, which makes the scheme very efficient.

RESULTS-DISCUSSION

Numerical Tests

Nonlinear Equation with Exact Solution

To assess the accuracy and convergence of our scheme we solve the nonlinear initial boundary value problem

$$\frac{\partial u}{\partial t} - \Delta u = uu_x + uu_y + f(x,y,t)\,, \quad (x,y;t) \in \mathring{\Omega} \times (0,T] \quad \text{where} \quad \Omega = [0,1]\times[0,1]\,, \tag{17}$$

$$f(x,y,t) = -2n\pi A^2 e^{-16n^2\pi^2 t} \sin(2n\pi x)\cos(2n\pi y)\cos[2n\pi(x+y)]\,, \tag{18}$$

$$u(0,y,t) = u(1,y,t) = 0 \ \text{ on } \ \partial\Omega_D \times (0,T] \ \text{ and } \ u(x,0,t) = u(x,1,t) \ \text{ on } \ \partial\Omega_P \times (0,T]\,, \tag{19}$$

$$u(x,y,0) = A\sin(2n\pi x)\cos(2n\pi y)\,,\ (x,y) \in \Omega\,, \tag{20}$$

which admits the exact analytic closed-form solution

$$U_{exact} = A\,\mathrm{e}^{-8n^2\pi^2 t}\sin(2n\pi x)\cos(2n\pi y)\,. \tag{21}$$

Problem (17)-(18), (19)-(20) is a good test case for our scheme because it has the same type of periodic and Dirichlet boundary conditions as the IBVP for the temperature and possesses a similar nonlinear term (see Eqs. (5),(6)-(7)).

To allow for a clearer presentation we use a uniform grid with mesh diameter $h = 1/2^{\mathcal{R}}$ where $\mathcal{R}$ is the number of mesh refinements. According to the theory the optimal L^2 error of the spatial approximation for *linear* problems is $\|U_{exact} - u_h\|_{L^2} = O(h^{q+1})$, where q is the degree of the basis functions [21, 22]. For the temporal approximation we use the θ method, which for $\lambda = 0.5$ is a second order method, *i.e.*, $\|U_{exact} - u_h\|_{L^2} = O(\Delta t^2)$ where Δt is the time step. Again, we underline that this is only true for *linear* equations. Therefore, for linear equations the overall error is given by

$$\|U_{exact} - u_h\|_{L^2} = O(h^{q+1}) + O(\Delta t^2)\,, \tag{22}$$

whereas for nonlinear equations a reduction in the order of accuracy is expected.

For the tests presented here the parameter valuers are $A = 2$, $n = 3$ and the final time T is $T = 0.25$. Linear polynomials are used ($q = 1$) and the time step is chosen as $\Delta t = h$ for the linear path and $\Delta t = h^2$ for the quadratic path. The results are presented in Table 1.

TABLE 1. Scheme Accuracy Test for Nonlinear IBVP.

	$\Delta t = h$		$\Delta t = h^2$	
h	$\|U_{exact}(\cdot,T) - u_h\|_\Omega$	Rate	$\|U_{exact}(\cdot,T) - u_h\|_\Omega$	Rate
2^{-6}	3.270772×10^{-03}	-	3.993340×10^{-8}	-
2^{-7}	2.876463×10^{-04}	3.50726	1.034621×10^{-8}	1.94849
2^{-8}	7.171584×10^{-05}	2.00393	2.616206×10^{-9}	1.98355
2^{-9}	1.792986×10^{-05}	1.99993	Did not perform	-

Let the L^2-error that corresponds to computation for a mesh with diameter $h = 1/2^{\mathcal{R}}$ be denoted by $err_{\mathcal{R}} = \|U_{exact}(\cdot,T) - u_h\|^{\mathcal{R}}_\Omega$. Then the rate is defined as the base two logarithm of the ratio $err_{\mathcal{R}}/err_{\mathcal{R}+1}$. Here we use linear polynomials as basis functions ($q = 1$) so the theoretical optimal error for the spatial approximation is $O(h^2)$. Therefore, the first column which represents the linear path is dominated by the temporal approximation and the second column (quadratic path) by the spatial approximation.

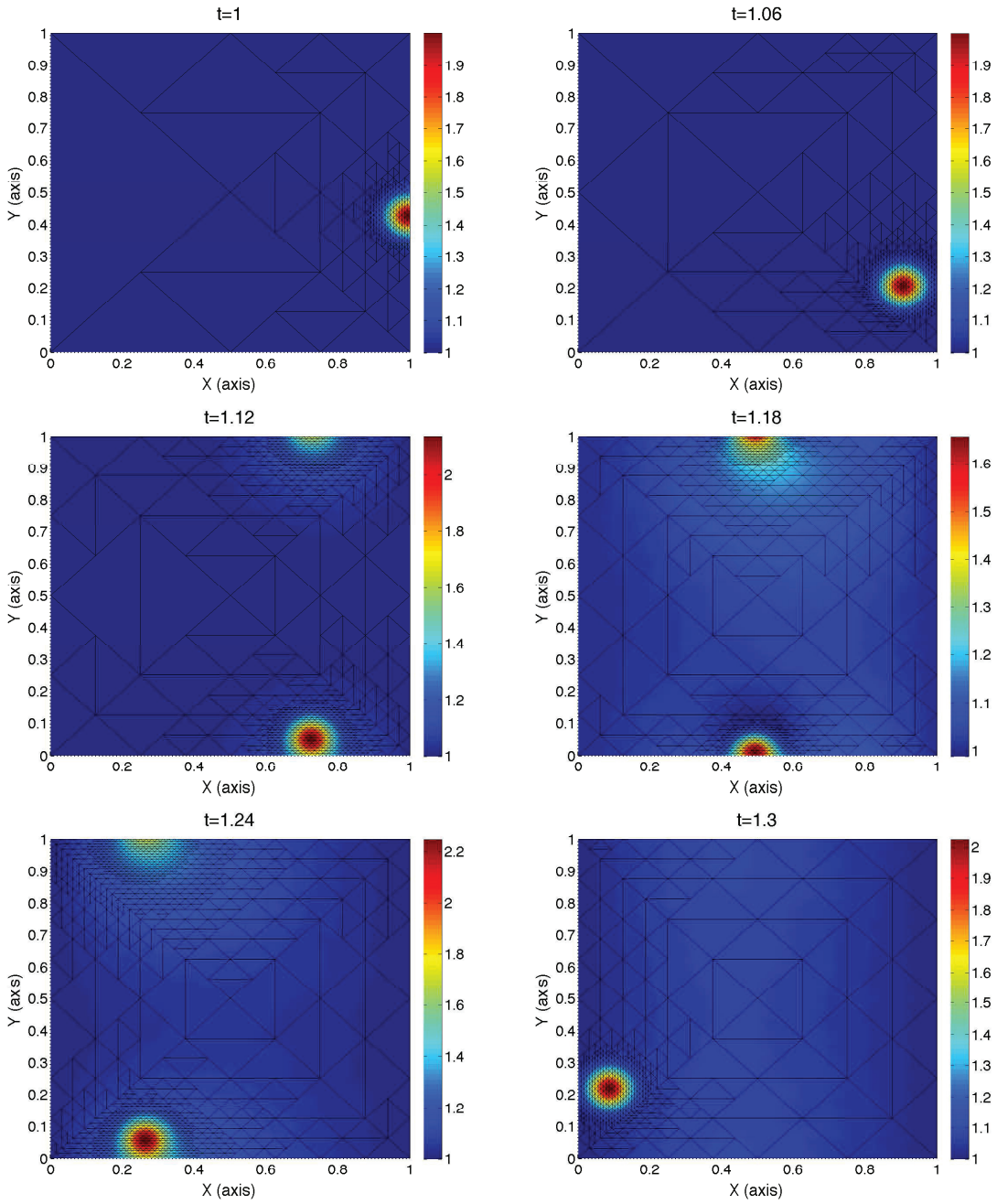

FIGURE 2. Solution of the moving ball problem for $a = 1$, $b = 2$ $c = 8$. The θ – method with $\theta = 0.5$ was used for the time discretization. Scheme parameters: Time step $\Delta t = 0.002$, refinement and coarsening constants $\Theta_R = 0.001$ and $\Theta_C = 0.0005$ respectively and basis function degree $q = 2$

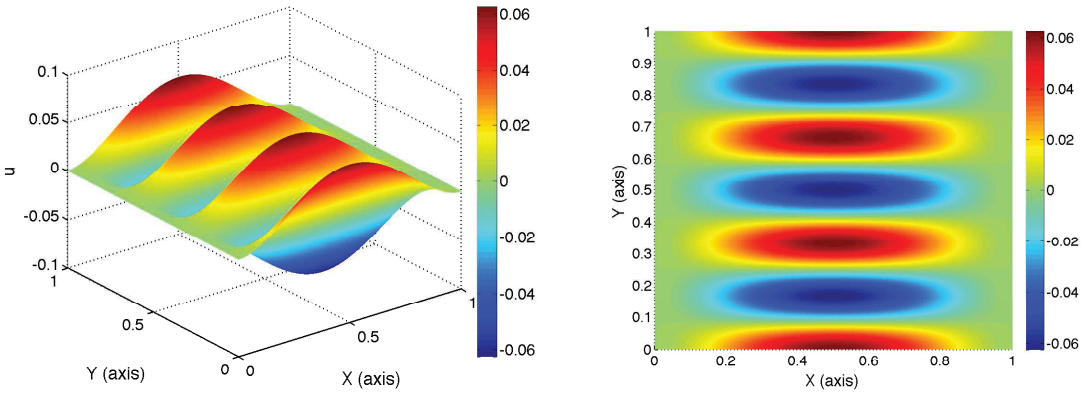

FIGURE 3. The numerical solution for stationary biharmonic test case. Left panel: Surface plot; Right panel: Density plot. The step-size used was $h = 1/2^4$ and the basis function degree was $q = 3$

Adaptivity - The "Moving Ball"

Our scheme is currently capable of performing adaptive coarsening and refinement for both stationary and time-dependent problems for any kind of boundary conditions, including periodic. To drive the adaptive mesh refinement and coarsening for our test problems, the Inverse Estimate Marking Strategy is used (see [26] and references therein). An appropriate marking strategy for the full problem of transient 2D convective flow (4)-(5), (6)-(7) is under investigation. The added difficulty comes from the fact that there are two unknown functions involved.

To describe the concepts involved we first define the following:

Definition 1 *For $u_h \in V_h^q$, at each element K we define*

$$c_K := h_K \frac{\|\nabla u_h\|_K}{\|u_h + a_K\|_K} \leq C \ , \tag{23}$$

where a_K an appropriately chosen constant to avoid division by zero and C an upper bound of c_K for all $K \in \mathcal{T}_h$ and all q.

Our marking strategy is based on the fact that the constants c_K are a measure of the spatial rate of change of the numerical solution u_h on a cell K. Large c_K values indicate a steep slope or oscillatory behavior. The marking criterion implemented in our algorithm is as follows:

Definition 2 *(The Inverse Estimate Marking Criterion)*
Let c_K, $K \in \mathcal{T}_h$ be the constants as defined in Eq. (23).

$$\textit{If } c_K \begin{cases} \leq & \Theta_C\, C \quad \textit{then coarsen.} \\ \geq & \Theta_R\, C \quad \textit{then refine.} \end{cases}$$

The constants Θ_C and Θ_R are problem specific and are chosen empirically.

The so-called moving ball problem is an excellent test for the adaptive capability of a scheme. It is a linear parabolic equation in two spatial dimensions whose solution profile is a circle (or ball) that moves in a circular manner. Appropriate changes to the signs and problem parameters can control the direction of motion and starting point. Here the ball starts at the right boundary and rotates in a clockwise direction.

The partial differential equation reads

$$\frac{\partial u}{\partial t} - \Delta u = f \, , \quad (x, y; t) \in \mathring{\Omega} \times (t_0, T] \tag{24}$$

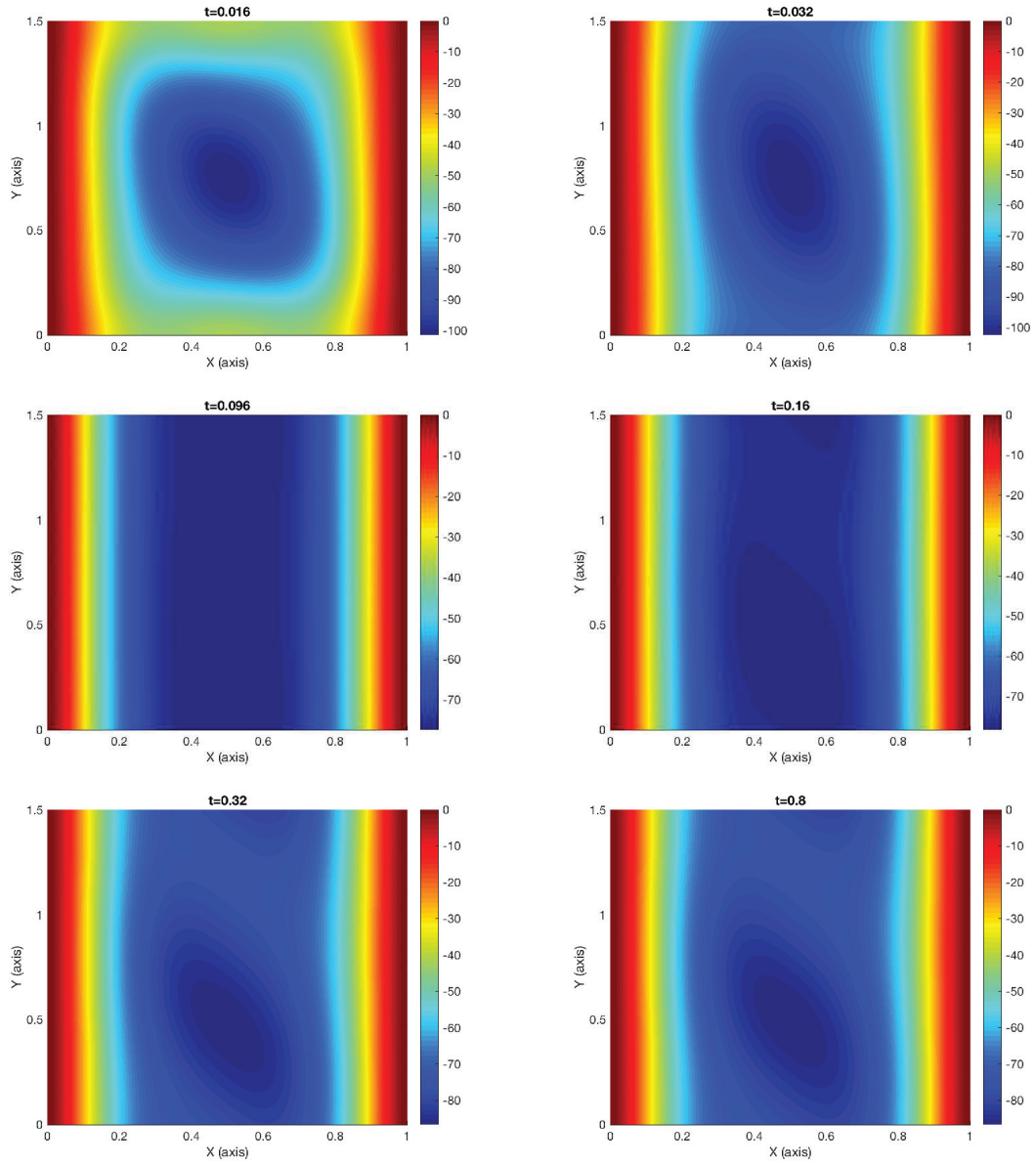

FIGURE 4. Transition to a standing wave for the case Pr = 1000, $\tau_B = 0.05461$ Ra = 3×10^5 ($\gamma = 8$). Selected snapshots of the streamfunction ψ. Scheme parameters: $q = 4$, $h = 1/16$, $T = 0.8$, $\Delta t = 8 \times 10^{-6}$.

where $\Omega = [0, 1] \times [0, 1]$ and

$$
\begin{aligned}
f = &\left\{600\frac{ac}{b}\left[\cos(ct)\left(-\frac{\sin(ct)}{b} + x - \frac{1}{2}\right) - \sin(ct)\left(-\frac{\cos(ct)}{b} + y - \frac{1}{2}\right)\right]\right. \\
&\left. + 1200a\left[1 - 75\left(1 - 2y + 2\frac{\cos(ct)}{b}\right)^2 - 75\left(1 - 2x + 2\frac{\sin(ct)}{b}\right)^2\right]\right\} \\
&\times \exp\left(-300\left[\left(-\frac{\cos(ct)}{b} + y - \frac{1}{2}\right)^2 + \left(-\frac{\sin(ct)}{b} + x - \frac{1}{2}\right)^2\right]\right).
\end{aligned} \tag{25}
$$

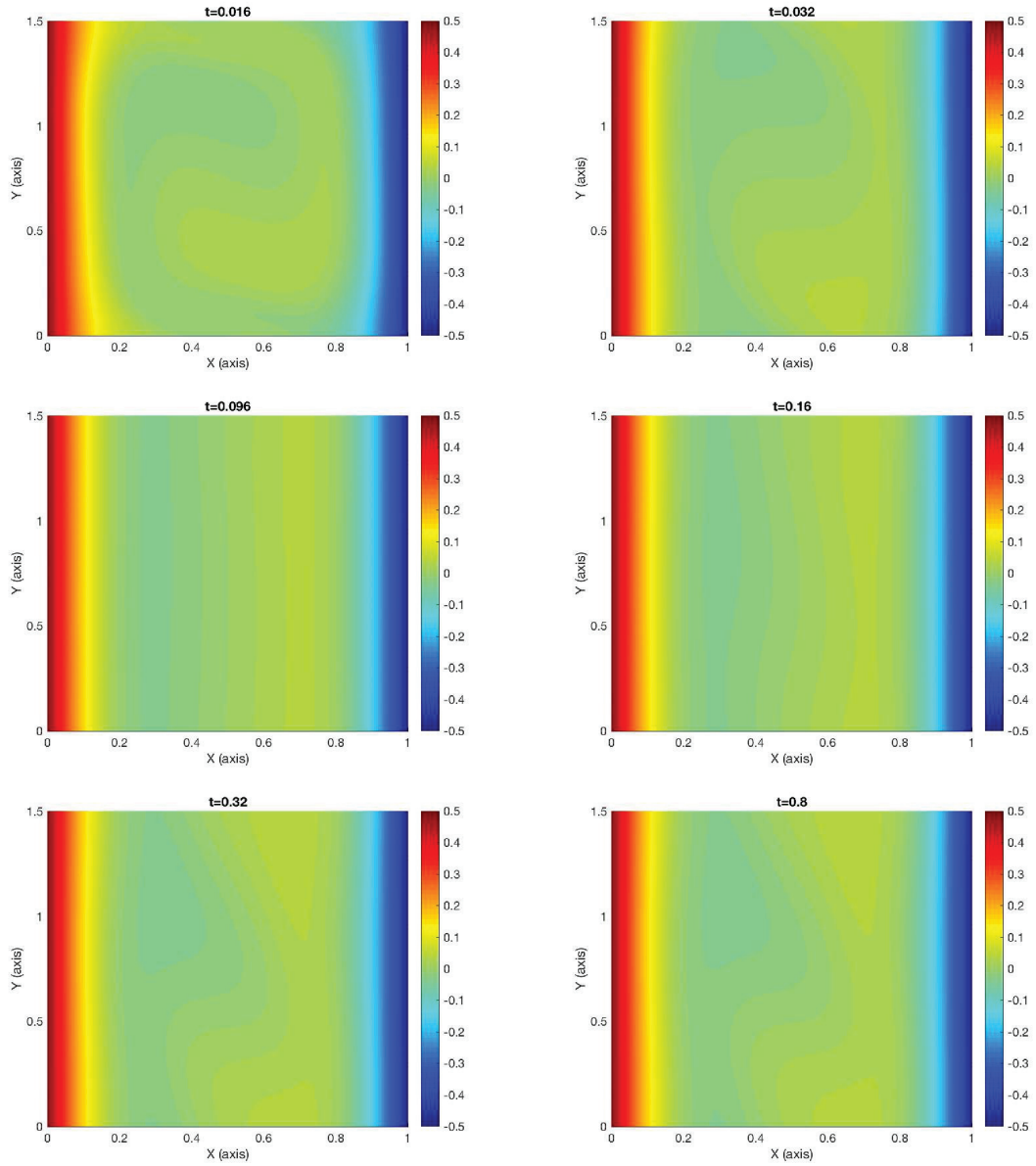

FIGURE 5. Transition to a standing wave for the case Pr = 1000, $\tau_B = 0.05461$ Ra = 3×10^5 ($\gamma = 8$). Selected snapshots of the temperature θ. The scheme parameters are the same as those in Figure 4.

Dirichlet conditions are prescribed at the left and right boundaries

$$u(x,0,t) = 1 + a\exp\left(-300\left[\left(-\frac{1}{2} - \frac{1}{b}\cos(ct)\right)^2 + \left(x - \frac{1}{2} - \frac{1}{b}\sin(ct)\right)^2\right]\right), \tag{26}$$

$$u(x,1,t) = 1 + a\exp\left(-300\left[\left(\frac{1}{2} - \frac{1}{b}\cos(ct)\right)^2 + \left(x - \frac{1}{2} - \frac{1}{b}\sin(ct)\right)^2\right]\right). \tag{27}$$

periodic conditions are applied at top and bottom boundaries,

$$u(x,0,t) = u(x,1,t) \ \text{ on } \ \partial\Omega_P \times (t_0, T] \tag{28}$$

and the initial condition is given by

$$u(x,y,t_0) = 1 + a\exp\left(-300\left[\left(y - \frac{1}{2} - \frac{1}{b}\cos(c\,t_0)\right)^2 + \left(x - \frac{1}{2} - \frac{1}{b}\sin(c\,t_0)\right)^2\right]\right),\ (x,y) \in \Omega\,. \tag{29}$$

We present our results for the case $a = 1$, $b = 2$, $c = 8$ in Figure 2. The initial condition is $t_0 = 1$. It was chosen in this way to avoid $t_0 = 0$ which represents a time where the "ball" would be touching a periodic boundary. The solution is superimposed on the mesh in order to clearly demonstrate how well it resolves the solution. It is clear that a much finer mesh follows the ball, which is a region where the solution gradient is high. The implementation of the periodic conditions imposed on the top and bottom boundaries is quite remarkable. When the ball touches one of the periodic boundaries its "missing" portion is mirrored in the opposite boundary. This behavior is followed by the mesh.

The biharmonic operator

The following fourth-order stationary boundary value problem demonstrates how well our method approximates the biharmonic operator and implements the periodic and homogeneous essential boundary conditions.

$$\Delta^2 u = f(x,y,t)\,, \quad (x,y) \in \mathring{\Omega} \ \text{ where } \ \Omega = [0,1]\times[0,1]\,, \tag{30}$$

$$f(x,y) = \left(162\,\pi^4 x^2(x-1)^2 - 18\,\pi^2(6x^2 - 6x + 1) + 3\right)8\cos(6\pi y)\,, \tag{31}$$

$$u(0,y) = u(1,y) = 0 \quad \text{on} \quad \partial\Omega_D \tag{32}$$

$$\text{and} \quad u(x,0) = u(x,1), \quad u_y(x,0,t) = u_y(x,H,t), \quad u_{yy}(x,0,t) = u_{yy}(x,H,t), \quad u_{yyy}(x,0,t) = u_{yyy}(x,H,t) \quad \text{on} \quad \partial\Omega_P.$$

This is especially important because the equation for the streamfunction contains the same biharmonic differential operator (4) and is subject to the exact same periodic (7) and homogeneous (6) boundary conditions. BVP (30)-(32) admits the exact solution

$$U_{exact} = x^2(x - 1.0)^2\cos(3\pi y)\,. \tag{33}$$

The results are presented in Figure 3. The correct implementation of the homogeneous Neumann boundary conditions can be easily seen in the surface plot (left panel) whereas the periodic nature of the solution and the homogeneous Dirichlet conditions are observed in both the surface and density plots of the numerical solution.

Results for the Two-Dimensional Flow

Our numerical results for the case Pr = 1000, Ra = 3×10^5, $\tau_B = 0.05461$, ($\gamma = 8$) and $H = 1.5$ are presented in Figure 4 and Fig. 5 for the streamfunction ψ_h and the temperature θ_h respectively. According to [14, 11] this set of parameter values corresponds to a standing wave (SW). Our computations confirm this conclusion, since after $t = 0.4$ which corresponds to time step $n_{SW} = 5000$ the maximum absolute difference between solutions at $t = n\Delta t$ and $t = (n + 200)\Delta t$ for $n \geq n_{SW}$ is less than 10^{-5} for ψ and 10^{-8} for θ. This is an even stricter criterion than comparing two consecutive time steps.

Figures 4 and 5 show the transition of the flow and temperature fields to a standing wave. The final time was $T = 0.8$ and for this value the streamfunction is near-identical to Figure 4.(a) of reference [14]; the corresponding plot for θ is not shown in [14]. We note here that the modes corresponding to the wavelength $H = 1.5$ are the most dangerous for this parameter set [15], which makes the agreement between our results and those of Christov and Homsy in [14] even more significant.

Another important feature is the thickness of boundary layer. According to the theory it should be equal to $1/\gamma$, where γ is the stratification parameter [14, 16]. In our case it is given by $1/\gamma = 0.125$, which is very near the results depicted in both Figure 4 and Figure 5. We would also like to point out that our computations were carried out with a rather coarse mesh ($h = 1/16$).

CONCLUSIONS

An accurate and efficient SIP-DG numerical method was developed for two-dimensional-in-space unsteady convective flows. For the spatial discretization, the SIP-DG approach was applied to both the streamfunction and temperature equations because of its innate ability to handle discontinuities and complex geometries. The resulting block-structured symmetric positive definite coefficient matrices allowed for the use of fast numerical solvers. In addition, due to the fact that the primal formulation was used, the algebraic system symmetry and positive-definiteness was maintained allowing for further efficiency. For the time discretization the θ-method was employed.

In addition to the problem of unsteady 2D convective flow, our method was applied to three boundary value problems which tested various features required of of our scheme: A nonlinear parabolic equation, a linear parabolic equation and a stationary biharmonic equation. All three test cases involved Dirichlet and periodic boundary equations whereas the biharmonic equation was subject to periodic and homogeneous essential conditions. The linear parabolic equation was solved with an adaptive mesh which resolved the solution very well. The results were found to be in agreement with the corresponding exact solutions where available.

The convective flow problem was solved for the case of a stationary wave. Despite the fact that the modes corresponding to wavelength $H = 1.5$ are rather volatile the agreement between our computations and published results was very good both for the streamfunction snapshot after the stationary wave is reached and the thickness of the boundary layer. We have therefore developed an efficient, accurate and flexible scheme which is a good platform for forming a numerical framework suitable for the investigation of more complex flows.

ACKNOWLEDGEMENTS

The work of N. C. Papanicolaou was partially supported by the Scientific Foundation of Republic of Bulgaria under grant DFNI I-02/9.

REFERENCES

[1] Y. Shu, B. Q. Li, and H. C. de Groh III (2002) *Numer. Heat Tr. A-Appl.* **42**, 345–364.
[2] A. C. Aristotelous, I. Klapper, Y. Grabovsky, B. Pabst, B. Pitts, and P. S. Stewart (2015) *Phys. Rev. E* **92**, 022703, 7p.
[3] A. C. Aristotelous and M. A. Haider (2014) *Int. J. Numer. Meth. Biomed. Eng.* **30**, 767–780.
[4] S. Simic-Stefani, M. Kawaji, and H. H. Hu (2006) *J. Cryst. Growth* **294**, 373–384.
[5] B. Straughan (2009) *Ricerche Mat.* **58**, 157–162.
[6] B. Straughan and F. Franchi (1984) *Proc. Roy. Soc. Edinb.* **96A**, 175–178.
[7] C. I. Christov (2009) *Mech. Res. Comm.* **36**, 481–486.
[8] S. Bargmann, P. Steinmann, and P. M. Jordan (2008) *Phys. Lett. A* **372**, 4418–4424.
[9] M. Ostoja-Starzewski (2009) *Int. J. Eng. Sci.* **47**, 807–810.
[10] N. Afrin, Y. Zhang, and J. K. Chen (2011) *Int. J. Heat Mass Transfer* **54**, 2419–2426.
[11] J. W. Elder (1965) *J. Fluid Mech.* **23**, 77–98.
[12] A. E. Gill and A. Davey (1969) *J. Fluid Mech.* **35**, 775–798.
[13] R. F. Bergholz (1978) *J. Fluid Mech.* **84**, 743–768.
[14] C. I. Christov and G. M. Homsy (2001) *J. Fluid Mech.* **430**, 335–360.
[15] X. H. Tang and C. I. Christov (2007) *Math. Comput. Simul.* **74**, 203–213.
[16] N. C. Papanicolaou, C. I. Christov, and G. M. Homsy (2009) *Int. J. Numer. Method Fluid* **59**, 945–965.
[17] N. C. Papanicolaou, C. I. Christov, and P. M. Jordan (2011) *Eur. J. Mech. B-Fluid* **30**, 68–75.
[18] N. C. Papanicolaou and A. C. Aristotelous, "High-order discontinuous Galerkin methods for coupled thermoconvective flows under gravity modulation," in *AMiTaNS'15*, AIP Conference Proceedings, Vol. 1684, edited by M.D. Todorov (American Institute of Physics, Melville, NY, 2015), Article 090010, 9p.
[19] T. Gudi, N. Nataraj, and A. K. Pani (2008) *J. Sci. Comput.* **37**, 139–161.
[20] K. Vemaganti (2007) *Num. Meth. PDE* **23**, 587–596.
[21] D. N. Arnold (1982) *SIAM J. Numer. Anal.* **19**, 742–760.
[22] D. N. Arnold, F. Brezzi, B. Cockburn, and L. D. Marini (2002) *SIAM J. Numer. Anal.* **39**, 1749–1779.
[23] I. Mozolevski, E. Süli, and P. R. Bösing (2007) *J. Sci. Comput.* **30**, 465–491.
[24] E. H. Georgoulis and P. Houston (2009) *IMA J. of Numer. Anal.* **29**, 573–594.
[25] G. A. Baker (1977) *Math. Comp.* **31**, 44–59.
[26] A. C. Aristotelous, O. A. Karakashian, and S. M. Wise (2015) *IMA J. Numer. Anal.* **35**, 1167–1198.